Published online April 27, 2005

Agronomy Journal

Volume 97 May–June 2005 Number 3

Temporal and Spatial Relationships between Within-Field Yield Variability in Cotton and High-Spatial Hyperspectral Remote Sensing Imagery

P. J. Zarco-Tejada,* S. L. Ustin, and M. L. Whiting

ABSTRACT

Traditional remote sensing methods for yield estimation rely on broadband vegetation indices, such as the Normalized Difference Vegetation Index, NDVI. Despite demonstrated relationships between such traditional indices and yield, NDVI saturates at larger leaf area index (LAI) values, and it is affected by soil background. We present results obtained with several new narrow-band hyperspectral indices calculated from the Airborne Visible and Near Infrared (AVNIR) hyperspectral sensor flown over a cotton (*Gossypium hirsutum* L.) field in California (USA) collected over an entire growing season at 1-m spatial resolution. Within-field variability of yield monitor spatial data collected during harvest was correlated with hyperspectral indices related to crop growth and canopy structure, chlorophyll concentration, and water content. The time-series of indices calculated from the imagery were assessed to understand within-field yield variability in cotton at different growth stages. A *K* means clustering method was used to perform field segmentation on hyperspectral indices in classes of low, medium, and high yield, and confusion matrices were used to calculate the kappa (κ) coefficient and overall accuracy. Structural indices related to LAI [Renormalized Difference Vegetation Index (RDVI), Modified Triangular Vegetation Index (MTVI), and Optimized Soil-Adjusted Vegetation Index (OSAVI)] obtained the best relationships with yield and field segmentation at early growth stages. Hyperspectral indices related to crop physiological status [Modified Chlorophyll Absorption Index (MCARI) and Transformed Chlorophyll Absorption Index (TCARI)] were superior at later growth stages, close to harvest. From confusion matrices and class analyses, the overall accuracy (and kappa) of RDVI at early stages was 61% (κ = 0.39), dropping to 39% (κ = 0.08) before harvest. The MCARI chlorophyll index remained sensitive to within-field yield variability at late preharvest stage, obtaining overall accuracy of 51% (κ = 0.22).

Remote sensing reflectance imagery provides spatial and temporal information on cotton plant growth and development (Plant et al., 2000). Traditionally, aerial photography and digital broadband multispectral sensors have been used to obtain remote sensing information in agriculture in the study of the relationships between red and near-infrared (NIR) reflectance and crop yield and development. During the development of the Landsat sensors, MSS and TM, spectral channels were selected to maximize the collection of agricultural and other vegetation indicators while minimizing the sensor payload and data download. Common methods to obtain spatial and temporal crop status based on these sensors rely on calculating vegetation indices such as the traditional NDVI. The NDVI is built on normalized red and NIR spectral bands, which are affected by both pigment absorption (red) and the scattering by the medium (NIR), a function of the arrangement of elements of the canopy (structure). Therefore, NDVI is sensitive to vegetation greenness and canopy scattering, causing its relationship with crop growth (Yuzhu, 1990; Benedetti and Rossini, 1993; Plant et al., 2000). For example, Plant et al. (2000) used false color infrared aerial photography to calculate NDVI, studying its relationship to cotton yield. Defoliation, boll opening, and regrowth control in cotton were evaluated with NDVI calculated from color infrared digital images (Yang et al., 2003), suggesting potential applications of remote sensing data for cotton defoliation strategies. In a different study, growth conditions and yield variation were mapped in cotton, sorghum [*Sorghum bicolor* (L.) Moench], and corn (*Zea mays* L.) using three spectral bands and four vegetation indices calculated from color infrared digital images (Yang et al., 2001), showing the applicability of remote sensing to study within-field variability and growth conditions. Other successful attempts to relate time series NDVI images calculated from digital color infrared data with spatial yield (Yang and Everitt, 2002) demonstrated that the best relationships occurred at the peak development

Cent. for Spatial Technol. and Remote Sensing (CSTARS), Dep. of Land, Air, and Water Resour. (LAWR), One Shields Ave., The Barn, Univ. of California, Davis, CA 95616-8671, USA. Received 20 Oct. 2003. Remote Sensing. *Corresponding author (pzarco@ias.csic.es).

Published in Agron. J. 97:641–653 (2005).
doi:10.2134/agronj2003.0257

677 S. Segoe Rd., Madison, WI 53711 USA

Abbreviations: AVNIR, Airborne Visible and Near Infrared; C_{a+b}, chlorophyll *a* and *b*; CARI, Chlorophyll Absorption in Reflectance Index; DGPS, differential global positioning system; LAI, leaf area index; MCARI, Modified Chlorophyll Absorption Index; MSAVI, Improved Soil-Adjusted Vegetation Index; MSR, Modified Simple Ratio; MTVI, Modified Triangular Vegetation Index; NDVI, Normalized Difference Vegetation Index; NDWI, Normalized Difference Water Index; NIR, near infrared; OSAVI, Optimized Soil-Adjusted Vegetation Index; PWI, Plant Water Index; RDVI, Renormalized Difference Vegetation Index; SAVI, Soil-Adjusted Vegetation Index; SRWI, Simple Ratio Water Index; TCARI, Transformed Chlorophyll Absorption Index; TVI, Triangular Vegetation Index.

stage in sorghum. In addition, the temporal stability of within-field cotton variation was studied with Landsat-TM imagery for 11 yr, demonstrating a strong degree of stability that enabled the use of temporal remote sensing imagery to derive regions of yield similarity (Boydell and McBratney, 2002). Several other studies showed high correlations between broadband NDVI and yield for different crops (Yuzhu, 1990; Benedetti and Rossini, 1993) through seasonal integration of NDVI (Denison et al., 1996; Wiegand et al., 1991) as well as by calculation of the fraction of absorbed photosynthetically active radiation (FPAR) from optical remote sensing measurements (Clevers, 1997).

Despite these successes for yield and crop status evaluation using the NDVI calculated from multispectral sensors, it is well documented that NDVI data saturate at high LAI values substantially below the LAI characteristic of high-productivity crops. The NDVI becomes saturated at LAI of 3 to 4 for most ecosystems (Sellers et al., 1986) while crop LAI often exceeds this value at peak development stages. The NDVI is especially affected by dense and multilayered canopies, showing a nonlinear relationship with green LAI (Lillesaeter, 1982; Baret and Guyot, 1991). Moreover, NDVI is affected by other factors such as soil background, canopy shadows, illumination, atmospheric conditions, and variation in leaf chlorophyll concentration, requiring uncoupling methods through simulation strategies to assess their impact on predicting green LAI (Haboudane et al., 2002, 2004).

New methods that use hyperspectral remote sensing enable the calculation of several other narrow-band vegetation indices related to biophysical and biochemical crop variables, suggested as potentially useful for precision agriculture (Deguise et al., 1999; Willis et al., 1999). Several new vegetation indices have been proposed that relate crop physiological status to hyperspectral data through their relationships to biochemical constituent concentrations, such as chlorophyll (Vogelmann et al., 1993; Carter, 1994; Gitelson and Merzlyak, 1996; Zarco-Tejada et al., 2001; Haboudane et al., 2002), carotenoids (Fuentes et al., 2001; Sims and Gamon 2002, 2003), water (Gao, 1996; Peñuelas et al., 1997), cellulose, lignin, and dry matter (Jacquemoud et al., 1996). These relationships are useful for obtaining information about the physiological and stress conditions that could potentially affect crop yield. Indices based on these biochemical attributes may produce more accurate predictive relationships that could be extended with greater confidence than broadband indicators. In addition, hyperspectral data enable calculation of narrow-band indices using combined spectral bands that minimize undesired background effects when estimating green LAI (Huete, 1988; Rondeaux et al., 1996). These hyperspectral vegetation indices perform better than traditional broadband indices (such as NDVI), avoiding saturation at high LAI (Haboudane et al., 2004). Therefore, hyperspectral remote sensing also enables the estimation of crop structural variables, such as LAI, which in addition to biochemical constituent estimation, may serve as robust indicators of crop development and physiological status for precision agriculture purposes, e.g., yield variability and field segmentation methods.

This study presents results obtained when comparing spatial cotton yield data, collected with a yield monitor, with narrow-band indices related to pigment concentration, canopy water content, LAI, and canopy structure. The temporal dependence of such narrow-band indices with yield as function of biochemical and biophysical information were studied for an entire growing season with airborne hyperspectral imagery collected bimonthly at 1-m spatial resolution. Field segmentation techniques to obtain homogeneous yield classes from hyperspectral indices were assessed using unsupervised clustering methods.

MATERIALS AND METHODS

Hyperspectral Remote Sensing Indices for Crop Status

A potential indicator of the status of vegetation stress is chlorophyll *a* and *b* (C_{a+b}) content because of its direct role in the photosynthetic processes of light harvesting and initiation of electron transport and its responsiveness to a range of crop stresses. In the chloroplast, light energy is harvested and processed by two functional units, Photosystem I and II, which produce oxygen and energy through a series of reduction–oxidation reactions to transport electrons. Stressed vegetation undergoes various physiological perturbations in the light-dependent reactions of photosynthesis, including disruption of electron transfer and structural damage to photosynthetic pigments. Differences between healthy and stressed vegetation in remotely sensed reflectance that are due to changes in C_{a+b} levels have been detected at the green peak (≈550 nm) and over the red edge spectral region (690 to 750 nm) (Rock et al., 1988; Vogelmann et al., 1993; Carter, 1994), thereby enabling the feasibility of remote detection of crop stress. Chlorophyll *a* and *b* and other leaf biochemical constituents such as dry matter and water content may be used as indicators of plant stress and nutritional deficiencies caused by N and other elements such as P, K, Fe, Ca, Mn, Zn, and Mg (Marschner et al., 1986; Fernández-Escobar et al., 1999; Jolley and Brown, 1999; Chen and Barak, 1982; Wallace, 1991; Tagliavini and Rombolà, 2001). Besides, the estimation of leaf N content at the canopy level from estimates of total chlorophyll concentration may be obtained because the majority of leaf N is contained in chlorophyll (Daughtry et al., 2000; Yoder and Pettigrew-Crosby, 1995) and ribulose-1-5-bisphosphate carboxylase/oxygenase (Rubisco) molecules (Evans, 1983; Evans and Seemann, 1989; Nakano et al., 1997; Woodrow and Berry, 1988). Many studies have demonstrated a direct relationship among the rate of photosynthesis, light absorbance, leaf N concentrations, and dry matter production (Alt et al., 2000). Monitoring canopy N from hyperspectral techniques has important implications for fertilization of agricultural crops and N deposition, which affects C storage and generates vegetation injury after prolonged N additions (Schulze et al., 1989) and increases N losses by gaseous and solute pathways in the C–N system. A management goal for agriculture is to supply adequate N while minimizing N losses (Daughtry et al., 2000) in the C–N system, besides limiting other economic and environmental effects (Rejesus and Hornbaker, 1999).

Attempts to remotely quantify total leaf N are confounded by the dynamic vertical distribution of N and chlorophyll within crop canopies, changes in LAI associated with fluctuations in N availability, and phenological shifts. While suboptimal canopy N is easily detectable in reduced chlorophyll concen-

Table 1. Vegetation indices for biochemical and leaf area index (LAI) estimation calculated from multispectral and hyperspectral imagery.

Vegetation index	Equation	Reference
	Structural indices	
Normalized Difference Vegetation Index (NDVI)	$NDVI = (R_{NIR} - R_{red})/(R_{NIR} + R_{red})$	Rouse et al. (1974)
Modified Triangular Vegetation Index (MTVI1)	$MTVI1 = 1.2 \times [1.2 \times (R_{800} - R_{550}) - 2.5 \times (R_{670} - R_{550})]$	Haboudane et al. (2004)
Modified Triangular Vegetation Index (MTVI2)	$MTVI2 = \frac{1.5 \times [1.2 \times (R_{800} - R_{550}) - 2.5 \times (R_{670} - R_{550})]}{\sqrt{(2 \times R_{800} + 1)^2 - (6 \times R_{800} - 5 \times \sqrt{R_{670}}) - 0.5}}$	Haboudane et al. (2004)
Renormalized Difference Vegetation Index (RDVI)	$RDVI = (R_{800} - R_{670})/\sqrt{(R_{800} + R_{670})}$	Rougean and Breon (1995)
Simple Ratio Index (SR)	$SR = R_{NIR}/R_{red}$	Jordan (1969); Rouse et al. (1974)
Modified Simple Ratio (MSR)	$MSR = \frac{R_{NIR}/R_{red} - 1}{(R_{NIR}/R_{red})^{0.5} + 1}$	Chen (1996)
Modified Chlorophyll Absorption in Reflectance Index ($MCARI_1$)	$MCARI1 = 1.2 \times [2.5 \times (R_{800} - R_{670}) - 1.3 \times (R_{800} - R_{550})]$	Haboudane et al. (2004)
Modified Chlorophyll Absorption in Reflectance Index ($MCARI_2$)	$MCARI2 = \frac{1.5 \times [2.5 \times (R_{800} - R_{670}) - 1.3 \times (R_{800} - R_{550})]}{\sqrt{(2 \times R_{800} + 1)^2 - (6 \times R_{800} - 5 \times \sqrt{R_{680}}) - 0.5}}$	Haboudane et al. (2004)
Soil Adjusted Vegetation Index (SAVI)	$SAVI = (1 + L) \times (R_{800} - R_{670})/(R_{800} + R_{670} + L)$ [$L \varepsilon (0,1)$]	Huete (1988); Qi et al. (1994)
Improved SAVI with self-adjustment factor L (MSAVI)	$MSAVI = \frac{1}{2}[2 \times R_{800} + 1 - \sqrt{(2 \times R_{800} + 1)^2 - 8 \times (R_{800} - R_{670})}]$	Qi et al. (1994)
Optimized Soil-Adjusted Vegetation Index (OSAVI)	$OSAVI = (1 + 0.16) \times (R_{800} - R_{670})/(R_{800} + R_{670} + 0.16)$	Rondeaux et al. (1996)
	Chlorophyll indices	
Greenness Index (G)	$G = R_{554}/R_{677}$	–
Modified Chlorophyll Absorption in Reflectance Index (MCARI)	$MCARI = [(R_{700} - R_{670}) - 0.2 \times (R_{700} - R_{550})] \times (R_{700}/R_{670})$	Daughtry et al. (2000)
Transformed CARI (TCARI)	$TCARI = 3 \times [(R_{700} - R_{670}) - 0.2 \times (R_{700} - R_{550}) \times (R_{700}/R_{670})]$	Haboudane et al. (2002)
Triangular Vegetation Index (TVI)	$TVI = 0.5 \times [120 \times (R_{750} - R_{550}) - 200 \times (R_{670} - R_{550})]$	Broge and Leblanc (2000)
Zarco-Tejada & Miller	$ZTM = R_{750}/R_{710}$	Zarco-Tejada et al. (2001)
	Water indices	
Normalized Difference Water Index (NDWI)	$NDWI = (R_{860} - R_{1240})/(R_{860} + R_{1240})$	Gao (1996)
Simple Ratio Water Index (SRWI)	$SRWI = R_{858}/R_{1240}$	Zarco-Tejada et al. (2003)
Plant Water Index (PWI)	$PWI = R_{970}/R_{900}$	Peñuelas et al. (1997)
	Red edge spectral parameters	
λ_p	$\lambda_{pr} = \lambda_{max(680-750)}$; $\lambda_{p1g} = \lambda_{max(500-600)}$; $\lambda_{p2g} = \lambda_{min(500-600)}$	Hare et al. (1984); Bonham-Carter (1988)
R_o	$R_o = R_{min(650-700)}$	Hare et al. (1984); Bonham-Carter (1988)
R_s	$R_s = R_{max(700-770)}$	Hare et al. (1984); Bonham-Carter (1988)
σ	σ = shape parameter as defined by the inverted-Gaussian curve-fit model	Hare et al. (1984); Bonham-Carter (1988)
	Other indices mentioned but not used in this study	
Simple Ratio Pigment Index (SRPI)	$SRPI = R_{430}/R_{680}$	Peñuelas et al. (1995)
Normalized Phaeophytinization Index (NPQI)	$NPQI = (R_{415} - R_{435})/(R_{415} + R_{435})$	Barnes (1992)
Photochemical Reflectance Index (PRI)	$PRI_1 = (R_{528} - R_{567})/(R_{528} + R_{567})$ $PRI_2 = (R_{531} - R_{570})/(R_{531} + R_{570})$	Gamon et al. (1992)
Normalized Pigment Chlorophyll Index (NPCI)	$NPCI = (R_{680} - R_{430})/(R_{680} + R_{430})$	Peñuelas et al. (1994)
Carter indices	$Ctr1 = R_{695}/R_{420}$ $Ctr2 = R_{695}/R_{760}$	Carter (1994); Carter et al. (1996)
Lichtenthaler indices	$Lic1 = (R_{800} - R_{680})/(R_{800} + R_{680})$; $Lic2 = R_{440}/R_{690}$; $Lic3 = R_{440}/R_{740}$; $Lic4 = \int_{450}^{680} R$	Lichtenthaler et al. (1996)
Structure Intensive Pigment Index (SIPI)	$SIPI = (R_{800} - R_{450})/(R_{800} + R_{650})$	Peñuelas et al. (1995)
Vogelmann indices	$Vog1 = R_{740}/R_{720}$; $Vog2 = (R_{734} - R_{747})/(R_{715} + R_{726})$; $Vog3 = (R_{734} - R_{747})/(R_{715} + R_{720})$;$Vog4 = D_{715}/D_{705}$	Vogelmann et al. (1993); Zarco-Tejada et al. (1999)
Gitelson and Merzlyak	$G\_M1 = R_{750}/R_{550}$ $G\_M2 = R_{750}/R_{700}$	Gitelson and Merzlyak (1997)
Curvature Index (Fluorescence)	$CUR = (R_{675} \cdot R_{690})/(R_{683}^2)$	Zarco-Tejada et al. (2000)
Double-Peak Ratio indices	$DPR1 = D_{\lambda p(680-750)}/D_{\lambda 0+12}$; $DPR2 = D_{\lambda p(680-750)}/D_{\lambda 0+22}$; $DP21 = D_{\lambda p(680-750)}/D_{703}$; $DP22 = D_{\lambda p(680-750)}/D_{720}$	Zarco-Tejada et al. (2001)
Area Red Edge Peak (ADR)	$ADR = \int_{680}^{760} D$	Zarco-Tejada et al. (2001)

tration (Schröder et al., 2000), excess N is poorly estimated by C_{a+b} concentration (Wood et al., 1993; Dwyer et al., 1995; Varvel et al., 1997). However, Blackmer et al. (1994) demonstrated that reflectance measured at 550 nm provided a good correlation between leaf N and chlorophyll determinations over a range of N availabilities from deficient to abundant.

Traditional broadband remote sensing methods for vegetation monitoring rely on the calculation of normalized indices such as NDVI, Simple Ratio Index, Modified Simple Ratio (MSR), and the Greenness Index as indicators of LAI, a critical parameter for estimating evapotranspiration, photosynthesis, primary productivity, and C cycling (Running et al., 1999).

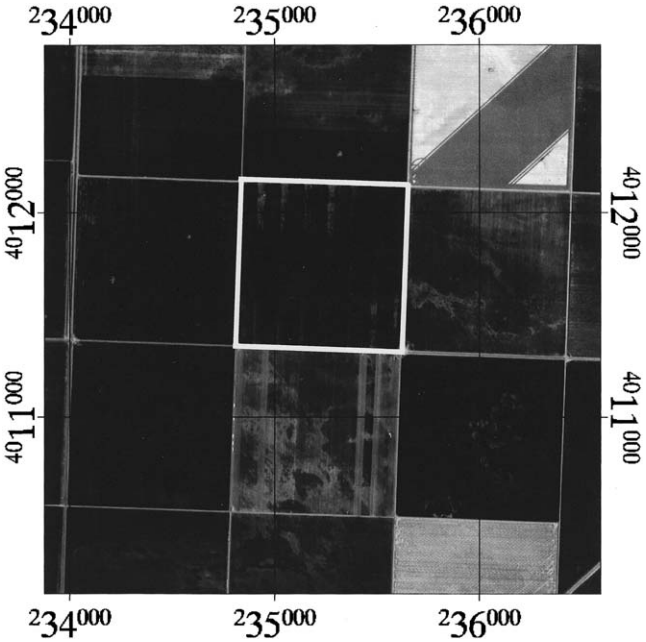

Fig. 1. Ikonos image obtained on 7 July 2001 showing the cotton field used for this study in upper center of the frame. The coordinate grid is Universal Transverse Mercator, Zone 11.

Leaf area index for many crops and forests often exceeds the saturated NDVI estimates for LAI (Sellers et al., 1986), making these predicted LAI greatly underestimate the fluxes of CO_2 and H_2O and inaccurately estimate biomass accumulation.

On the other hand, several hyperspectral indices track and quantify chlorophyll concentration (Vogelmann et al., 1993; Gitelson and Merzlyak, 1997; Carter, 1994; Zarco-Tejada et al., 2001), allowing remote detection of vegetation stress and mapping through the chlorophyll content variation (Zarco-Tejada et al., 1999). These physiologically based vegetation indices are, among others (see Zarco-Tejada, 2000, and Zarco-Tejada et al., 2001, for a full review) (Table 1), visible ratios such as the Simple Ratio Pigment Index (SRPI), the Normalized Phaeophytinization Index (NPQI), the Photochemical Reflectance Index (PRI), Normalized Pigment Chlorophyll Index (NPCI), Carter indices, the Greenness Index (G), Lichtenthaler indices in the visible/NIR, and the Structure Intensive Pigment Index (SIPI). Ratio indices of red edge reflectance calculated in the 690- to 750-nm region are Vogelmann indices, Gitelson & Merzylak, Carter, Curvature Index, and calculation of the area of the derivative under the red edge. Finally, spectral and derivative red edge indices are the red edge inflection wavelengths and maximum chlorophyll depth wavelength, λ_p and λ_o, respectively, and the shape parameter (σ) using inverted Gaussian curve fitting of the red edge (Miller et al., 1990), as well as other spectral indices calculated from derivative analysis such as the double-peak indices DPR1, DPR2, DP21, and DP22 (Zarco-Tejada et al., 2001).

In agricultural canopies, with large spectral contributions by the soil background and LAI variation in different growth stages, combined indices have been proposed to minimize background soil effects while maximizing sensitivity to C_{a+b}. The Chlorophyll Absorption in Reflectance Index (CARI) (Kim et al., 1994) was shown to reduce the variability of photosynthetically active radiation due to nonphotosynthetic materials. The MCARI (Daughtry et al., 2000) was a modification of CARI to minimize the combined effects of the soil reflectance and the nonphotosynthetic materials. The Soil-Adjusted

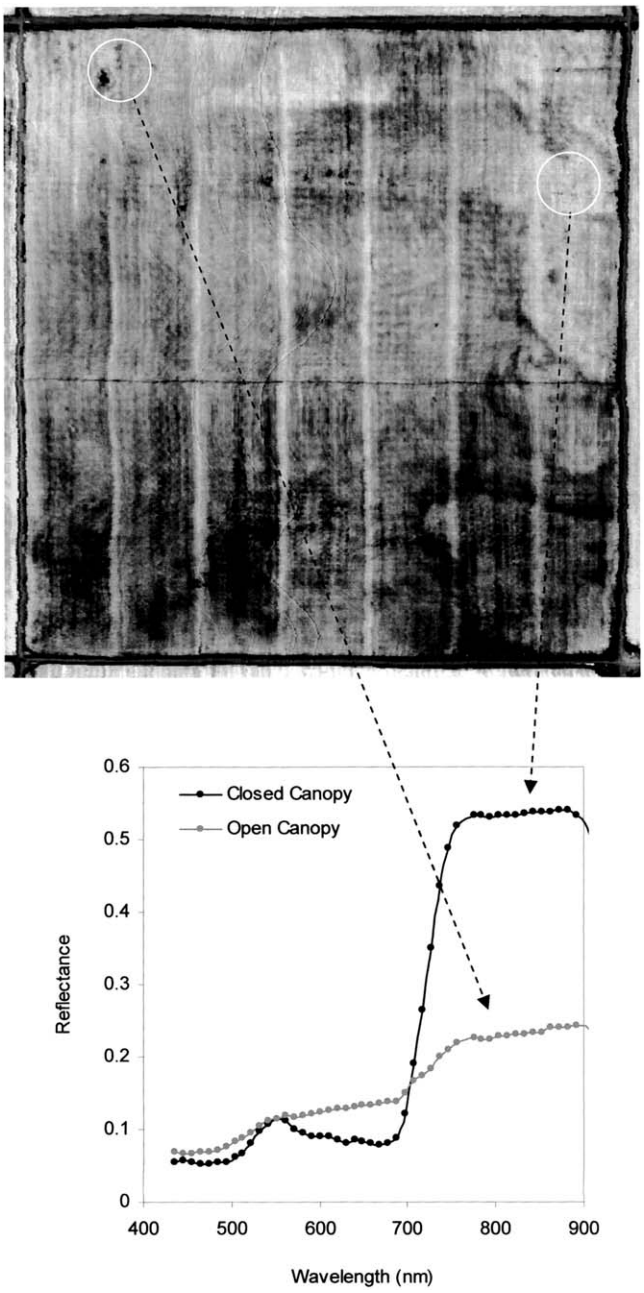

Fig. 3. Reflectance spectral measurements obtained from the airborne image showing two areas of low and high growth. This black and white reproduction is of a AVNIR image color composite of band centers at 454.92, 455.00, and 804.12 nm.

Vegetation Index (SAVI) (Huete, 1988) and OSAVI (Rondeaux et al., 1996) were proposed as soil-line vegetation indices that could be combined with MCARI to reduce contributions from background reflectance (Daughtry et al., 2000). As an example, C_{a+b} was successfully estimated for corn canopies at different growth stages using the combined TCARI/OSAVI index, proving its robustness to LAI and background influence variations (Haboudane et al., 2002).

Besides estimating C_{a+b} concentration, several studies demonstrated the existing link between leaf-level reflectance over the 400- to 2500-nm spectral region and the amount of water in the leaf through optical indices, regression analysis, and radiative transfer modeling (Gausman et al., 1970; Allen et al., 1971; Hunt et al., 1987; Carter, 1991, 1993; Danson et al., 1992;

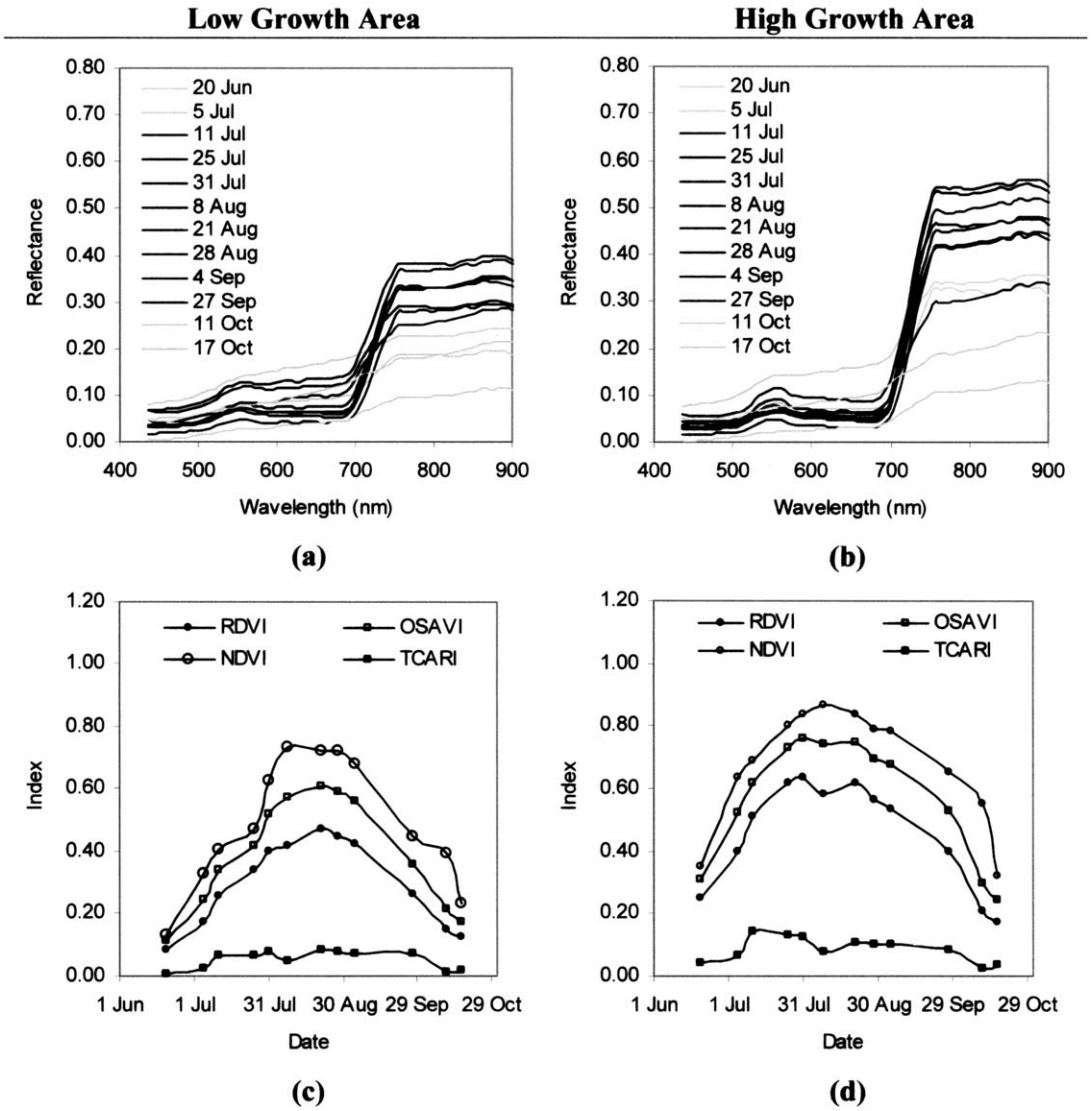

Fig. 4. Time series of (a and b) hyperspectral reflectance and (c and d) chlorophyll-related indices (TCARI), leaf area index related indices (RDVI and NDVI), and OSAVI calculated for areas of (a and c) low and (b and d) high growth development for the entire growing season.

Aldakheel and Danson, 1997; Jacquemoud and Baret, 1990; Ceccato et al., 2001). The effects of water content on leaf reflectance were studied by Carter (1991), who showed that sensitivity to water content was greatest in spectral bands centered at 1450, 1940, and 2500 nm where liquid water has major absorption features. Indirect effects of water content on reflectance were also found at 400 nm and in the red edge at 700 nm (Filella and Peñuelas, 1994). Other studies demonstrated that leaf-level optical indices and ratios centered at the secondary water absorption bands at 940 and 1200 nm obtained good correlation with leaf water thickness (Ustin et al., 1998; Gao and Goetz, 1995). Peñuelas et al. (1997) developed the Plant Water Index (PWI, R_{970}/R_{900}), Gao (1996) developed the Normalized Difference Water Index (NDWI) calculated as $(R_{860}-R_{1240})/(R_{860}+R_{1240})$ and Zarco-Tejada et al. (2003) the Simple Ratio Water Index (SRWI, R_{858}/R_{1240}).

Other indices developed to avoid saturation at high LAI levels and yet be sensitive to chlorophyll concentration changes were also tested in this study. These indices, such as MTVI2 and MCARI2 among others (Table 1), are discussed in depth in Haboudane et al. (2004).

Hyperspectral Airborne Acquisitions and Field Data Collection

Cotton Study Site Selection

The cotton study site was located on the western side of the northern San Joaquin Valley of California, USA. This highly fertile region is well known as a top producer of cotton, garlic (*Allium sativum* L.), tomato (*Lycopersicon esculentum* Mill.), pistachio (*Pistacia vera* L.), alfalfa (*Medicago sativa* L.), hay, and grain. The site is a NASA/USDA Ag20/20 Demonstration Precision Agriculture research site, located near the city of Lemoore in Kings County. This Ag20/20 cotton project involves collaborative research from University of California–Davis, University of California Cooperative Extension and Field Stations agents, USDA, farm advisors, and commercial vendors in precision agriculture. The cotton field of interest is 36.6° N lat and 120.0° W long, denoted in the upper center of an Ikonos image collected in July 2001 (Fig. 1).

The soils in the study area formed in alluvial deposits from Cretaceous marine sediments of the California Coast Range to the west and alluvium from the Kings River emanating

Table 2. Correlation coefficients calculated between hyperspectral indices and within-field yield data for all images acquired during the growing season.

Index	20 June	5 July	11 July	25 July	31 July	8 Aug.	21 Aug.	28 Aug.	4 Sept.	27 Sept.	11 Oct.	17 Oct.
Structural indices												
NDVI	0.54	0.59	*0.61*	0.56	0.56	0.48	0.46	0.45	0.45	0.22	0.01	0.06
MTVI1	0.59	0.57	*0.60*	0.57	0.55	0.51	0.49	0.47	0.47	0.20	0.04	0.10
MTVI2	0.59	0.59	*0.61*	0.57	0.56	0.51	0.49	0.47	0.47	0.20	0.03	0.09
RDVI	0.59	*0.61*	*0.61*	0.58	0.53	0.52	0.49	0.48	0.47	0.22	0.03	0.10
SR	0.49	0.56	*0.59*	0.54	0.56	0.48	0.46	0.45	0.43	0.22	0.01	0.05
MSR	0.51	0.57	*0.60*	0.55	0.57	0.49	0.47	0.46	0.44	0.22	0.01	0.06
MCARI1	0.59	0.57	*0.60*	0.57	0.55	0.51	0.49	0.47	0.47	0.21	0.05	0.13
MCARI2	0.59	0.58	*0.60*	0.57	0.56	0.51	0.49	0.47	0.47	0.22	0.05	0.14
OSAVI	0.57	0.61	*0.61*	0.57	0.58	0.51	0.48	0.48	0.47	0.22	0.03	0.09
MSAVI	0.59	0.59	*0.61*	0.57	0.57	0.51	0.49	0.48	0.47	0.22	0.05	0.12
Chlorophyll indices												
R_{750}/R_{710}	0.55	0.50	0.56	0.56	*0.57*	0.49	0.48	0.43	0.40	0.04	−0.08	0.03
G	0.37	0.48	*0.58*	0.51	0.55	0.44	0.42	0.41	0.40	0.07	−0.05	−0.02
MCARI	0.51	*0.56*	0.52	0.52	0.54	0.47	0.43	0.45	0.47	*0.43*	0.27	0.08
TCARI	0.52	*0.57*	0.50	0.52	0.52	0.47	0.44	0.45	0.48	*0.41*	0.27	0.08
TCARI/OSAVI	*0.43*	0.42	0.03	0.18	0.24	0.33	0.13	0.18	0.19	0.20	0.29	0.07
TVI	*0.59*	0.57	*0.60*	0.56	0.54	0.51	0.48	0.47	0.47	0.17	0.02	0.06
C_{a+b} *f*(TCARI/OSAVI)	−0.02	−0.31	−0.06	−0.15	−0.09	−0.28	−0.09	−0.13	−0.11	−0.11	*−0.29*	−0.07
Water indices												
mNDWI	0.06	0.07	0.15	*0.19*	0.17	0.16	*0.19*	0.13	0.11	−0.14	−0.09	−0.14
mSRWI	0.06	0.06	0.15	*0.19*	0.17	0.15	*0.19*	0.13	0.11	−0.14	−0.08	−0.14
PWI	0.02	0.14	0.30	*0.35*	0.37	0.32	0.33	0.31	0.30	0.03	−0.07	−0.12
Red edge spectral parameters												
λ_o	0.02	0.40	0.34	*0.52*	0.08	0.40	0.42	0.40	0.34	0.00	−0.09	0.00
λ_p	−0.05	0.07	0.26	*0.34*	0.04	0.29	0.34	0.29	0.19	−0.09	−0.14	0.08
R_o	−0.23	−0.22	−0.50	*−0.52*	*−0.52*	−0.42	−0.42	−0.33	−0.41	−0.22	0.02	0.04
R_s	0.41	0.41	0.50	*0.52*	0.50	0.50	0.47	0.46	0.45	0.13	0.11	0.28
σ	−0.05	−0.16	0.10	*−0.31*	−0.25	−0.26	−0.19	−0.28	−0.27	−0.13	−0.07	0.08
Combination indices												
LAI (MCARI2)·C_{ab} *f*(TC/OS)	0.01	0.50	*0.52*	0.49	0.49	0.48	0.45	0.42	0.42	0.08	−0.10	0.01
LAI (MTVI2)	0.55	0.53	*0.55*	0.48	0.47	0.46	0.44	0.42	0.44	0.20	0.03	0.08
LAI (MCARI2)	*0.56*	0.52	0.55	0.48	0.47	0.46	0.44	0.42	0.44	0.22	0.04	0.12
LAI (MTVI2)·C_{ab} *f*(TC/OS)	0.01	0.51	*0.52*	0.49	0.49	0.47	0.45	0.42	0.42	0.08	−0.10	0.00
MCARI2·(TCARI/OSAVI)	0.54	*0.56*	0.51	0.53	0.51	0.47	0.45	0.46	0.48	0.41	0.27	0.10
MCARI2/(TCARI/OSAVI)	0.00	0.08	0.25	0.28	0.33	0.28	*0.47*	0.35	0.27	0.01	−0.09	0.00
NDVI·(TCARI/OSAVI)	0.51	*0.56*	0.50	0.50	0.52	0.46	0.42	0.43	0.47	0.40	0.24	0.07
NDVI·(TCARI/OSAVI)·PWI	0.50	*0.55*	0.53	0.50	0.51	0.45	0.42	0.43	0.47	0.39	0.20	0.05
MCARI·(TCARI/OSAVI)·PWI	0.54	*0.55*	0.54	0.52	0.50	0.46	0.44	0.45	0.48	0.39	0.23	0.09

from the Sierra Nevada mountain range to the east in aridic and aquic soil moisture regimes. Hydrology strongly influences soil characteristics in the region. In many areas, including the study site, perched ground water over deep clay layers transports salts from the upper alluvial fans and concentrates them in the lower fans, basin, and basin rim, requiring precision water and drainage management. The soils in the studied field are clay loam surfaces of coarse-loamy, mixed (calcareous), thermic Typic Torriorthents and fine, montmorillonitic, thermic Typic Natragrids. They are very deep, well-drained and moderately well-drained soils though the permeability is very slow or moderately slow (USDA-NRCS, 1978).

Cotton Yield and Management Data Collection

Yield data were collected at harvest using a cotton yield monitor (Model AG700, AGRIplan, Stow, MA, USA; www.agriplaninc.com; verified 28 Jan. 2005). The monitor measures the flow of the cotton in the chute using infrared light beams, calculating the momentary yield for the differential global positioning system (DGPS) position. The accuracy of the yield estimates range from 95 and 98%, measured in the field in the calibration process and validated with trials conducted simultaneously. The DGPS positions were instantaneously differentiated with Wide Area Augmentation System (WAAS) data for submeter accuracy. The yield pixel width is a function of the number and width of the cotton rows picked by harvester, with the yield weight averaged over the pixel width and a length of 1- to 5-s increments of DGPS collection, which is integrated with the speed of the harvester. The yield pixels were approximately 4.5 m^2. The yield and position data were displayed as raster maps using manufacturer-supplied mapping software in the on-board computer and downloaded as ASCII text and database files. The instantaneous yield data are shown in Fig. 2 (see page 650), revealing the spatial variability in yield.

In addition to yield data, the grower provided detailed information on farming practices, including fertilizer and irrigation schedules. Fertilizer recommendations and applications were based on soil and petiole testing for maximum yields and applied to the entire field. Irrigation was applied every 2 to 3 wk depending on the outcome of frequent leaf water retention pressure measurements, which were timed to reduce stress during the growing season. The last irrigation was applied on 18 Aug. 2001, before the 21 Oct. 2001 harvest.

Airborne Hyperspectral Imagery Acquisition

An airborne campaign was conducted at bimonthly intervals from June until October 2001 with the AVNIR hyperspectral sensor (OKSI, Inc., Torrance, CA, USA). The AVNIR images acquired at 1500 m above ground level obtained 1-m spatial resolution with 60 bands, covering the 430- to 1012-nm spectral range at 10-nm bandwidth. The sensor provided 652 cross-track pixels at 12 bits of radiometric resolution. A total of 12 images were acquired over the 2001 growing season, with

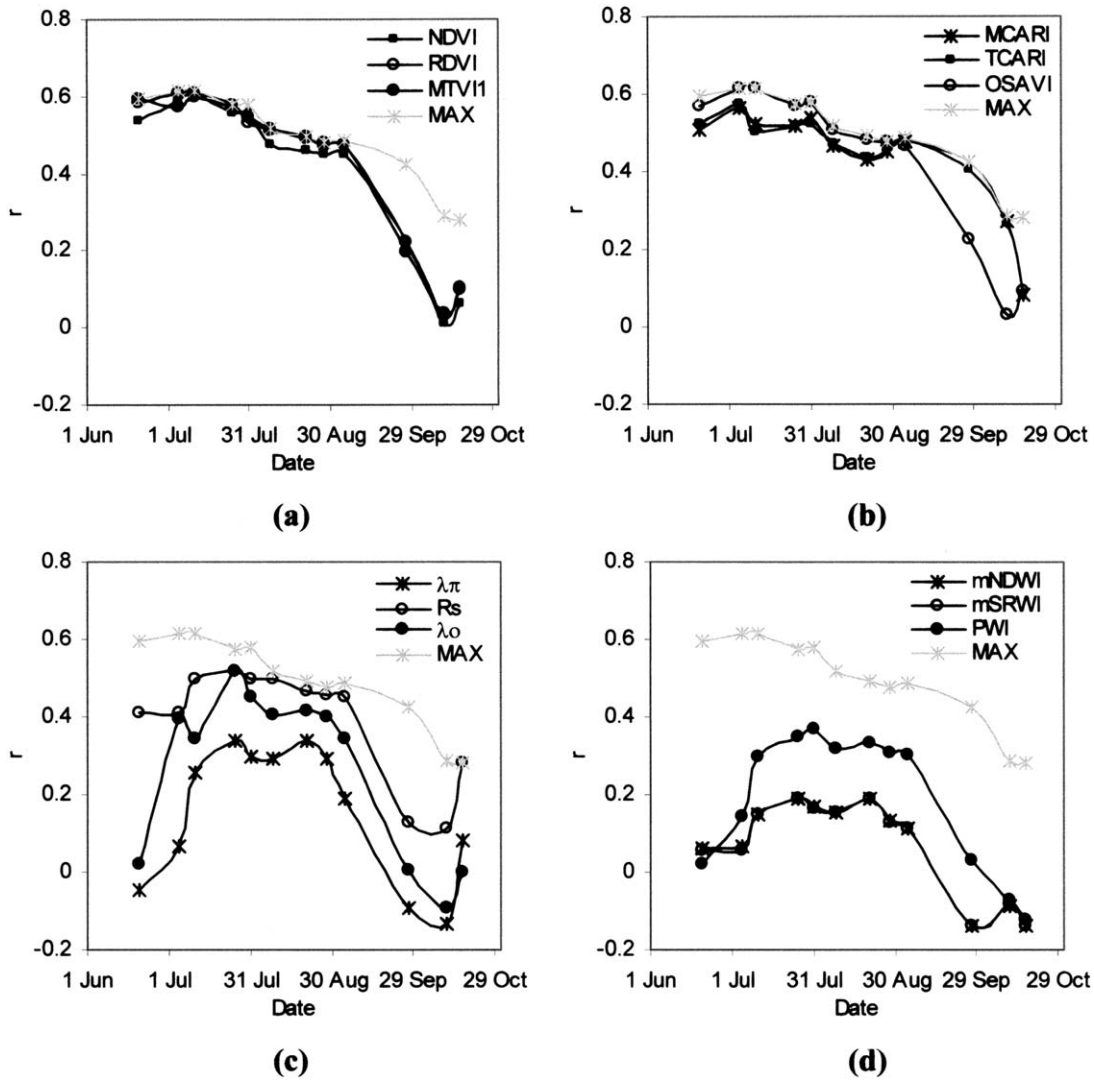

Fig. 5. Correlation coefficients (*r*) obtained between spatial yield data and hyperspectral indices as function of time. The best correlation coefficient for any index is labeled MAX compared with indices (a) NDVI, RDVI, and MTVI1; (b) MCARI, TCARI, and OSAVI; (c) red edge parameters λ_p, λ_o, and R_s; and (d) water indices PWI, mNDWI, mSRWI.

dates 20 June, 5 July, 11 July, 25 July, 31 July, 8 Aug., 21 Aug., 28 Aug., 4 Sept., 27 Sept., 11 Oct., and 17 Oct. Imagery was processed to *at-sensor* radiance, and atmospheric calibration was performed using the empirical line method with white and black reference calibration panels located immediately outside the field. Images were georeferenced and registered using four white panels placed at the corners of the field with submeter DGPS locations. Geometric distortions in the airborne imagery are normally due to variations in altitude and attitude (roll, pitch, and yaw) at the time of data acquisition. More than 100 ground control points were collected from each image at field boundaries and ground features inside the fields, using a thin plate spline transformation for registration and obtaining a georeferencing error less than the pixel size (1 m). Data sets registered to a common source of ground control points allowed comparison among hyperspectral imagery acquired on separate dates and the spatial yield image. A time series of hyperspectral imagery was produced that enabled a temporal study of the full spectra of each pixel and the calculation of vegetation indices at 1-m spatial resolution.

The poor and healthy growth stands within the field were captured by the imagery (Fig. 3), allowing spatial extraction of spectral reflectance and index calculations. Low growth areas were a mixture of stunted vegetation and soil background, greatly diminishing the reflectance due to the aggregation of vegetation, soil, and shadow components at this open canopy stage. Areas of advanced development at the closed-canopy stage did not exhibit soil background effects in the spectra and had higher reflectance in the NIR and lower reflectance in the visible region than open canopies due to the higher chlorophyll and carotenoid absorptions. The spectra and indices from these locations, when sequenced by date, let us study the effects of crop development and growth stage throughout the growing season on the hyperspectral signatures.

Analysis Methods

Coregistered multidate hyperspectral images and the spatial yield data, collected at harvest and resampled to a common 1-m pixel size, were compared. Image processing and statistical analysis were conducted using ENVI 3.6 software (Research Systems, Inc., Boulder, CO, USA).

A selection of 34 hyperspectral indices related to LAI, C_{a+b} (therefore, a potential indicator of leaf N status), canopy water

Table 3. Kappa (κ) and overall accuracy (%) obtained between airborne hyperspectral imagery and yield spatial data using *K* means classification clustering method into three classes of low, medium, and high yield.

Index	20 June	5 July	11 July	25 July	31 July	8 Aug.	21 Aug.	28 Aug.	4 Sept.	27 Sept.	11 Oct.	17 Oct.
	kappa (κ)											
NDVI	0.28	*0.36*	*0.36*	0.30	0.30	0.11	0.15	0.19	0.20	0.08	−0.01	−0.01
RDVI	0.35	*0.39*	*0.39*	0.34	0.30	0.27	0.26	0.25	0.26	0.08	0.00	0.00
MCARI	0.28	*0.34*	0.28	0.27	0.31	0.22	0.21	0.24	0.27	*0.22*	0.13	0.01
PWI	0.01	0.03	0.12	*0.15*	*0.15*	0.13	0.14	0.12	0.11	0.00	−0.03	−0.04
OSAVI	0.33	*0.40*	0.38	0.33	0.34	0.24	0.24	0.25	0.24	0.08	0.00	0.00
NDVI, RDVI, PWI, OSAVI	0.31	*0.40*	0.37	0.33	0.36	0.24	0.24	0.25	0.24	0.08	−0.01	−0.01
60 bands	0.09	0.14	*0.28*	0.25	0.25	0.25	0.24	0.22	0.23	0.14	0.16	0.16
	overall accuracy, %											
NDVI	53.80	58.60	*58.97*	54.43	54.41	39.84	43.04	46.42	46.69	39.42	33.21	31.72
RDVI	58.09	61.01	*61.24*	58.14	56.00	53.18	52.64	52.26	52.27	39.85	33.89	33.07
MCARI	53.90	*57.59*	53.66	53.14	55.64	50.71	49.09	51.28	52.98	*50.71*	43.37	35.36
PWI	36.00	35.70	43.12	45.11	*46.00*	44.83	45.09	43.78	42.82	35.52	33.56	32.98
OSAVI	56.97	*61.93*	60.48	56.91	57.90	50.57	49.86	51.67	50.14	39.74	33.94	32.55
NDVI, RDVI, PWI, OSAVI	55.85	*61.64*	60.21	56.80	58.74	50.51	50.20	51.70	50.18	39.41	33.33	32.80
60 bands	41.12	42.94	*53.91*	51.48	52.08	52.47	50.69	49.74	50.10	42.66	43.30	46.22

content, and red edge parameters were calculated from the hyperspectral reflectance images (Table 1). A time series of reflectance spectra and hyperspectral indices were derived from the imagery for representative areas of high and low growth, showing the effects of crop development and growth stage on the hyperspectral signature. Variation in hyperspectral reflectance, chlorophyll-related indices (TCARI), LAI-related indices (RDVI and NDVI), and OSAVI were calculated for these areas of low- and high-growth development (Fig. 3) over the entire growing season (Fig. 4). The lower NIR reflectance and a decrease in absorption in the visible spectrum after the last irrigation were due to reductions in green vegetation and a corresponding increase in the dry matter of the cotton canopy before harvest.

Coefficients from correlation analysis were obtained from comparison of the within-field spatial yield data and each calculated index on each acquisition date over the growing season (Table 2). The best indices for obtaining yield variability information in cotton were assessed, producing a time dependence for specific indices.

To study the capability of the proposed indices for deriving within-field areas of homogeneous yield, an unsupervised *K*-means method was applied to the spatial yield data and all hyperspectral image indices. The *K*-means unsupervised classification method calculates initial class means that are evenly distributed in the data space, iteratively clustering the pixels into the nearest class using a minimum distance technique (Tou and González, 1974). A total of three classes were obtained using the *K*-means clustering method, deriving areas of high, medium, and low yield. Confusion matrices were calculated for all index images, combinations of indices, and individual reflectance bands using the yield data set as the ground truth. The confusion matrix, overall accuracy value, and the kappa (κ) coefficient, which gives an overall accuracy assessment for the classification based on commission and omission errors for all classes (Richards, 1994), were calculated to evaluate the index performance and the appropriate time for the best separation of the field into management zones as function of yield variability.

RESULTS AND DISCUSSION

Correlation coefficients (r) obtained between all hyperspectral indices and yield data for all images acquired over the entire season are shown in Table 2. Results indicate that the relationships obtained between vegetation indices and spatial yield data varied over time, obtaining the best relationships in early growth stages between 5 and 11 July. At later stages, less strong relationships between yield and the vegetation indices were found, suggesting that within-field yield variability may be captured with remote sensing indices at early stages of development. The best relationships with yield (with $r > 0.6$) were found for indices MTVI1, MTVI2, RDVI, MSR, NDVI, TVI (Triangular Vegetation Index), MCARI1, MCARI2, OSAVI, and MSAVI (improved SAVI). Water-based indices and red edge indices did not perform well, obtaining lower success ($r < 0.4$). Combined indices between structural and chlorophyll indices, such as NDVI · (TCARI/OSAVI), did not obtain better results than single indices alone. Among the red edge spectral parameters, λ_o and R_s produced the best results ($r = 0.5$) but were inferior in all cases to OSAVI, MCARI, or RDVI indices.

Figure 5 shows the maximum correlation coefficient among the indices obtained for each image date (labeled as MAX) as well as indices NDVI, RDVI, and MTVI1 (Fig. 5a); MCARI, TCARI, and OSAVI (Fig. 5b); λ_p, λ_o, and R_s (Fig. 5c); and PWI, modified NDWI (mNDWI), and modified SRWI (mSRWI) (Fig. 5d). Table 2 and Fig. 5a and Fig. 5b indicate that structural indices related to LAI (NDVI, RDVI, and MTVI1) and OSAVI obtained better results at earlier and middle growth stages (until 30 August). At later stages, from the 4 Sept. date until harvest, structural indices such as NDVI poorly captured the yield variability, with low correlation coefficients reduced due to canopy dry down and defoliant application (Table 2). At such an advanced growth stage, chlorophyll indices such as MCARI and TCARI performed better because they do not appear to be as sensitive to the loss of turgor and leaf drop (Fig. 5b). The differential behavior of indices as function of time and, therefore, to different growth stages may indicate that structural indices related to canopy light scattering and growth are better indicators of spatial yield variability at early stages while chlorophyll-related indices are more suitable closer to harvest.

The ground-truth spatial yield image collected with the yield monitor and the images of hyperspectral indices calculated for each date in the time series were used for field segmentation. Results of κ and overall accuracy calculated between segmented field for each vegetation

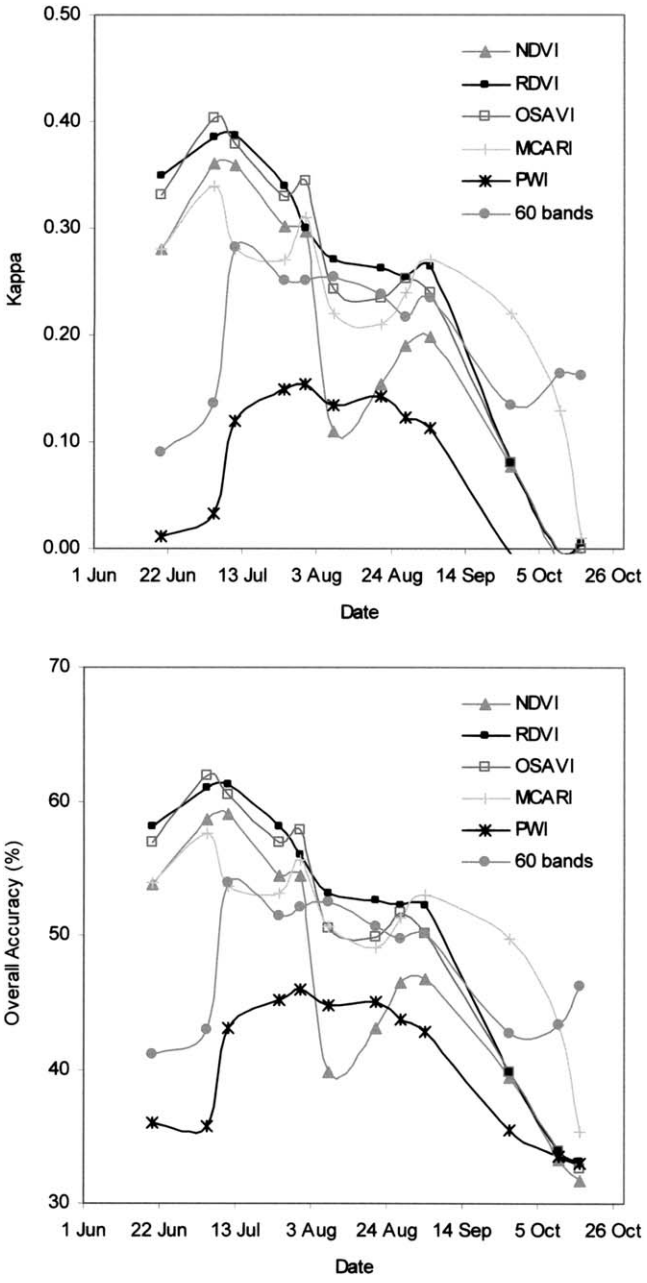

Fig. 6. Kappa coefficient (κ) and overall accuracy calculated between segmented yield image data and airborne imagery from spectral indices using an unsupervised *K*-means clustering method to produce low-, medium-, and high-yield classes.

index and ground-truth yield classes are shown in Table 3 and Fig. 6 for a selected set of the best-performing indices. The RDVI and OSAVI indices produced the best results, with overall accuracy greater than 60% and $\kappa = 0.4$. Water indices did not perform well for segmenting the field, obtaining $\kappa = 0.1$ with the PWI, indicating that water indices are not good indicators of yield variability. Better results were obtained in all cases with optical indices than with the 60 absolute reflectance bands used as input for the segmentation method ($\kappa = 0.4$ with RDVI vs. $\kappa = 0.14$ with the 60 absolute reflectance bands). Chlorophyll indices such as MCARI again obtained the best performance for field segmentation at later stages close to harvest, being superior to NDVI and structural indices at such advanced growth (on 27 Sept., results were $\kappa = 0.22$ and 50.7% accuracy with MCARI vs. $\kappa = 0.01$ and 39.4% accuracy with NDVI). The segmentation accuracy decreased with time for OSAVI and RDVI; nevertheless, they obtained better segmentation accuracies than the NDVI index (Fig. 6). The three yield classes are shown for the ground-truth image (Fig. 7a), from the 60 reflectance bands (Fig. 7b), NDVI (Fig. 7c), and OSAVI (Fig. 7d) at the time of maximum accuracy (5 July). The close visual agreement between ground-measured yield monitor classes and OSAVI classes can be seen, yielding better results than when NDVI is used for segmentation. A large overestimation of classes and poor field segmentation were obtained with direct comparison of reflectance bands, demonstrating that hyperspectral indices built on specific bands related to crop condition were better suited in this experiment for segmenting the field into zones of homogeneous yields due to their lower sensitivity to undesirable effects through normalizing the image.

The κ and overall accuracies shown in Table 3 demonstrate that the accuracies for the field segmentation of homogeneous yield classes are time dependent. The variation in class size and distribution by date for the OSAVI index segmentation is shown in Fig. 8 compared with homogeneous classes calculated from the spatial yield image. It suggests that a large variation of class size and distribution is a function of the time of acquisition, with better agreement between index-derived classes and within-field yield variability at earlier and middle growth stages.

CONCLUSIONS

This study indicates that new hyperspectral indices related to vegetation structure and canopy chlorophyll concentration provide complementary information about within-field yield variability to traditionally used indices, such as NDVI. Results show that the relationships between hyperspectral indices and spatial yield variability depend on the time of image acquisition, with the best relationships at mid- and earlier growth stages. Within-field yield variability was best captured at earlier stages with indices MTVI1, MTVI2, NDVI, RDVI, MSR, TVI, MCARI1, MCARI2, OSAVI, MCARI and MSAVI, with water-based indices and red edge indices performing poorly. It suggests that water content indices are unable to capture canopy variability related to cotton yield spatial distribution. Structural indices related to LAI (NDVI, RDVI, MTVI1, OSAVI) obtained better results at earlier and middle growth stages than at later stages before harvesting. At advanced growth stages and preharvest, chlorophyll-related indices such as MCARI and TCARI were better indicators of canopy heterogeneity associated with yield variability. The behavior of indices as a function of growth stage indicate that structural indices related to canopy scattering and growth are better indicators of field variability at earlier stages,

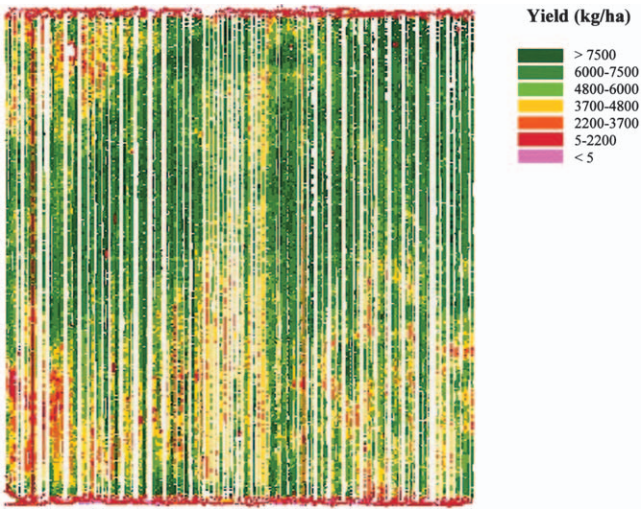

Fig. 2. Yield image for the cotton field, collected by the AGRIplan AG700 yield monitor, at 4.5-m spatial resolution.

with chlorophyll-related indices more suitable at stages closer to harvest.

The unsupervised *K*-means clustering technique used to test field segmentation methods with different hyperspectral indices and reflectance bands produced three classes of potentially low, medium, and high yield. Classes obtained from the different spectral indices were compared with yield classes using a confusion matrix that calculated the overall accuracy and kappa coefficient for assessment. The RDVI and OSAVI indices obtained the best results for field segmentation in homogeneous yield classes, with overall accuracy > 60% and $\kappa = 0.4$ while water indices performed poorly ($\kappa = 0.1$). Better results were obtained with optical indices when used as inputs for the classification, demonstrating that indices are superior to absolute reflectance bands for field segmentation. Optical indices have the advantage of minimizing undesirable effects through normalizing the image although in some cases, the indices alone may prevent the use of information from other spectral regions not used in the calculation of the index. At advanced growth stages close to harvest, chlorophyll indices such as MCARI produced the best performance for field segmentation and better captured the yield variability, being superior to structural indices related to LAI.

This research, using a temporal data set of hyperspectral imagery over the entire season, indicates that the accuracies for the field segmentation into zones of homogeneous yield are, as expected, time dependent, showing the time dependence of different indices as the cotton crop develops. Although similar relationships be-

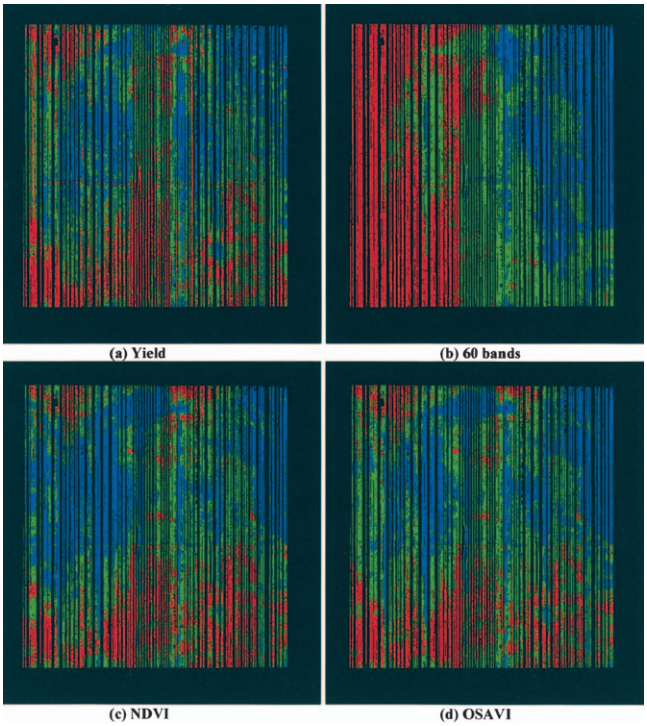

Fig. 7. Unsupervised *K* means clustering method for low (red)-, medium (green)-, and high (blue)-yield classes calculated from the hyperspectral airborne image that obtained the highest correlation with yield (5 July 2001). It shows better performance for OSAVI than NDVI index, with poor segmentation performance when 60 absolute reflectance bands are used. Airborne image pixels shown are only those where yield data were collected with the yield monitor.

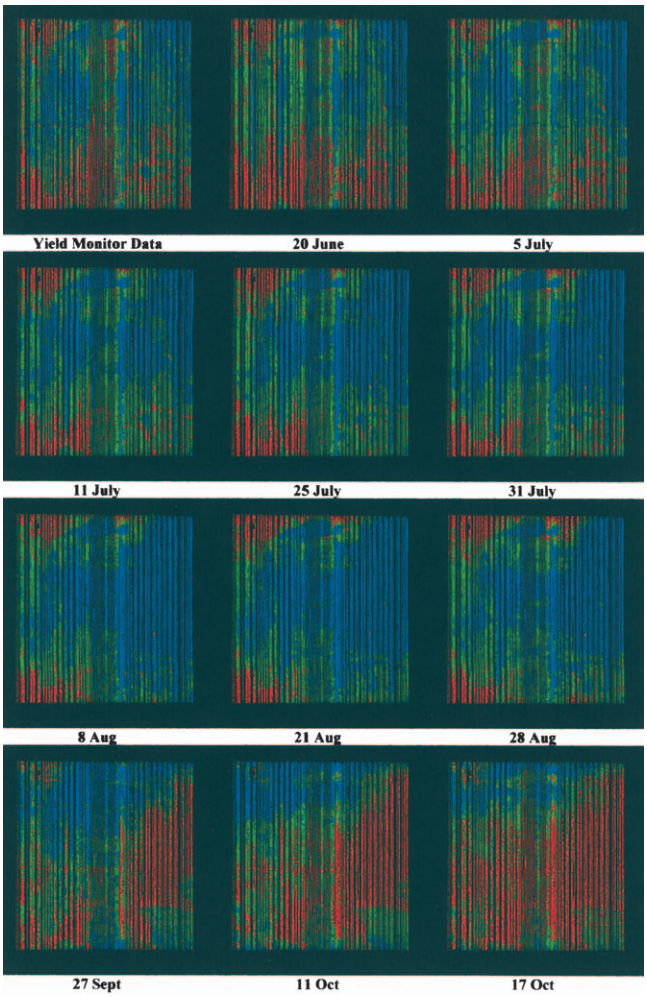

Fig. 8. Time series of segmented imagery using the OSAVI index for low (red)-, medium (green)-, and high (blue)-yield through *K*-means method, enabling the visual comparison with classes calculated from the spatial yield data. Airborne image pixels shown are only those where yield data were collected with the yield monitor.

tween yield and traditional indices (NDVI) and newly developed hyperspectral indices (RDVI and MTVI) were found, this work shows that hyperspectral indices add complementary information when the aim is to produce homogeneous yield management zones. Moreover, it indicates that new narrow-band hyperspectral indices such as RDVI and MTVI, related to LAI, perform better for field segmentation than NDVI indices that saturate at low LAI. Conclusions of this research to test the behavior of newer hyperspectral indices indicate that structural indices related to LAI (RDVI, MTVI, and OSAVI) were slightly superior to NDVI, producing the best relationships with yield and field segmentation at early growth stages. New hyperspectral indices related to chlorophyll status (MCARI and TCARI) better captured the within-field variability at later growth stages close to harvest, at which structural indices were not sensitive to spatial yield variability. This study may serve as a demonstration for the use of new indices calculated from hyperspectral imagery for precision agriculture management. These new methods have potential applications in identifying within-field variability as function of canopy structure and chlorophyll stress status for field segmentation purposes.

ACKNOWLEDGMENTS

The authors gratefully acknowledge the NASA/USDA jointly funded AG20/20 project for funding image acquisitions. Additional support for field data collection was provided by the National Cotton Foundation. Financial support provided for this research to P.J. Zarco-Tejada through the California Space Institute, NASA Space Grant Program, and the *Ramón y Cajal* (MCyT) and *Averroes* (JA) programs are gratefully acknowledged. We thank C. Rueda for computational code development needed for image processing and I. Kautter for image processing support.

REFERENCES

Aldakheel, Y.Y., and F.M. Danson. 1997. Spectral reflectance of dehydrating leaves: Measurements and modeling. Int. J. Remote Sens. 18:3683–3690.

Allen, W.A., H.W. Gausman, A.J. Richardson, and R. Cardenas. 1971. Water and air changes in grapefruit, corn and cotton leaves with maturation. Agron. J. 63:392–394.

Alt, C., H. Stutzel, and H. Kage. 2000. Optimal nitrogen content and photosynthesis in cauliflower (*Brassica oleracea* L. *botrytis*). Scaling up from leaf to whole plant. Ann. Bot. (London) 85:779–787.

Baret, F., and G. Guyot. 1991. Potentials and limits of vegetation indices for LAI and APAR assessment. Remote Sens. Environ. 35:161–173.

Barnes, J.D. 1992. A reappraisal of the use of DMSO for the extraction and determination of chlorophylls *a* and *b* in lichens and higher plants. Environ. Exp. Bot. 2:85–100.

Benedetti, R., and P. Rossini. 1993. On the use of NDVI profiles as a tool for agricultural statistics: The case study of wheat yield estimate and forecast in Emilia Romagna. Remote Sens. Environ. 45(3):311–326.

Blackmer, T.M., J.S. Schepers, and G.E. Varvel. 1994. Light reflectance compared with other nitrogen stress measurements in corn leaves. Agron. J. 86:934–938.

Bonham-Carter, G.F. 1988. Numerical procedures and computer program for fitting an inverted Gaussian Model to vegetation reflectance data. Comput. Geosci. 14:339–356.

Boydell, B., and A.B. McBratney. 2002. Identifying potential within-field management zones from cotton-yield estimates. Precis. Agric. 3:9–23.

Broge, N.H., and E. Leblanc. 2000. Comparing prediction power and stability of broadband and hyperspectral vegetation indices for estimation of green leaf area index and canopy chlorophyll density. Remote Sens. Environ. 76:156–172.

Carter, G.A. 1991. Primary and secondary effects of water content of the spectral reflectance of leaves. Am. J. Bot. 78:916–924.

Carter, G.A. 1993. Responses of leaf spectral reflectance to plant stress. Am. J. Bot. 80:239–243.

Carter, G.A. 1994. Ratios of leaf reflectances in narrow wavebands as indicators of plant stress. Int. J. Remote Sens. 15:697–704.

Carter, G.A., T.R. Dell, and W.G. Cibula. 1996. Spectral reflectance characteristics and digital imagery of a pine needle blight in the southeastern United States. Can. J. For. Res. 26:402–407.

Ceccato, P., S. Flasse, S. Tarantola, S. Jacquemoud, and J.M. Gregoire. 2001. Detecting vegetation leaf water content using reflectance in the optical domain. Remote Sens. Environ. 77:22–33.

Chen, J. 1996. Evaluation of vegetation indices and modified simple ratio for boreal applications. Can. J. Remote Sens. 22:229–242.

Chen, Y., and P. Barak. 1982. Iron nutrition of plants in calcareous soils. Adv. Agron. 35:217–240.

Clevers, J.G.P.W. 1997. A simplified approach for yield prediction of sugar beet based on optical remote sensing data. Remote Sens. Environ. 61:221–228.

Danson, F.M., M.D. Steven, T.J. Malthus, and J.A. Clarck. 1992. High-spectral resolution data for determining leaf water content. Int. J. Remote Sens. 13:461–470.

Daughtry, C.S.T., C.L. Walthall, M.S. Kim, E. Brown de Colstoun, and J.E. McMurtrey III. 2000. Estimating corn leaf chlorophyll concentration from leaf and canopy reflectance. Remote Sens. Environ. 74:229–239.

Deguise, J.C., M. McGovern, H. McNaim, and K. Staenz. 1999. Spatial high resolution crop measurements with airborne hyperspectral remote sensing. p. 1603–1608. *In* P.C. Robert et al. (ed.) Precision agriculture. Proc. Int. Conf., 4th, St. Paul, MN. 19–22 July 1998. ASA, CSSA, and SSSA, Madison, WI.

Denison, R.F., R.O. Miller, D. Bryant, A. Abshahi, and W.E. Wildman. 1996. Image processing extracts more information from color infrared aerial photographs. Calif. Agric. 50(3):9–13.

Dwyer, L.M., A.M. Anderson, B.L. Ma, and D.W. Stewart. 1995. Quantifying the nonlinearity in chlorophyll meter response to corn leaf nitrogen concentration. Can. J. Plant Sci. 75:179–182.

Evans, J.R. 1983. Nitrogen and photosynthesis in the flag leaf of wheat (*Triticum aestivum* L.). Plant Physiol. 72:759–302.

Evans, J.R., and J.R. Seemann. 1989. The allocation of protein N in the photosynthetic apparatus: Costs, consequences and control. p. 183–205. *In* W.R. Briggs (ed.) Photosynthesis. Alan R. Liss, New York.

Fernández-Escobar, R., R. Moreno, and M. Garcia-Creus. 1999. Seasonal changes of mineral nutrients in olive leaves during the alternate-bearing cycle. Sci. Hortic. 82:24–45.

Filella, I., and J. Peñuelas. 1994. The red edge position and shape as indicators of plant chlorophyll content, biomass and hydric status. Int. J. Remote Sens. 15:1459–1470.

Fuentes, D.A., J.A. Gamon, H.-L. Qiu, D.A. Sims, and D.A. Roberts. 2001. Mapping Canadian boreal forest vegetation using pigment and water absorption features derived from the AVIRIS sensor. J. Geophys. Res. 106(D24):33,565–33,577.

Gamon, J.A., J. Peñuelas, and C.B. Field. 1992. A narrow-waveband spectral index that tracks diurnal changes in photosynthetic efficiency. Remote Sens. Environ. 41:35–44.

Gao, B.-C. 1996. NDWI—a normalized difference water index for remote sensing of vegetation liquid water from space. Remote Sens. Environ. 58:257–266.

Gao, B.-C., and A.F.H. Goetz. 1995. Retrieval of equivalent water thickness and information related to biochemical components of vegetation canopies from AVIRIS data. Remote Sens. Environ. 52:155–162.

Gausman, H.W., W.A. Allen, R. Cardenas, and A.J. Richarson. 1970. Relation of light reflectance to histological and physical evaluations of cotton leaf maturity. Appl. Opt. 9:545–552.

Gitelson, A.A., and M.N. Merzlyak. 1996. Signature analysis of leaf reflectance spectra: Algorithm development for remote sensing of chlorophyll. J. Plant Physiol. 148:494–500.

Gitelson, A.A., and M.N. Merzlyak. 1997. Remote estimation of chlo-

rophyll content in higher plant leaves. Int. J. Remote Sens. 18: 2691–2697.

Haboudane, D., J.R. Miller, E. Pattey, P.J. Zarco-Tejada, and I. Strachan. 2004. Hyperspectral vegetation indices and novel algorithms for predicting green LAI of crop canopies: Modeling and validation in the context of precision agriculture. Remote Sens. Environ. 90: 337–352.

Haboudane, D., J.R. Miller, N. Tremblay, P.J. Zarco-Tejada, and L. Dextraze. 2002. Integration of hyperspectral vegetation indices for prediction of crop chlorophyll content for application to precision agriculture. Remote Sens. Environ. 81(2–3):416–426.

Hare, E.W., J.R. Miller, and G.R. Edwards. 1984. Studies of the vegetation red reflectance edge in geobotanical remote sensing. p. 433–440. *In* Proc. Canadian Symp. on Remote Sensing, 9th, St. John's, NF. 13–17 Aug. 1984. Canadian Remote Sens. Soc., Canadian Aeronautics and Space Inst., Ottawa, ON.

Huete, A.R. 1988. A soil-adjusted vegetation index (SAVI). Remote Sens. Environ. 25:295–309.

Hunt, E.R., B.N. Rock, and P.S. Nobel. 1987. Measurement of leaf relative water content by infrared reflectance. Remote Sens. Environ. 22:429–435.

Jacquemoud, S., and F. Baret. 1990. Prospect: A model of leaf optical properties spectra. Remote Sens. Environ. 34:75–91.

Jacquemoud, S., S.L. Ustin, J. Verdebout, G. Schmuck, G. Andreoli, and B. Hosgood. 1996. Estimating leaf biochemistry using the PROSPECT leaf optical properties model. Remote Sens. Environ. 56:194–202.

Jolley, V.D., and J.C. Brown. 1999. Genetically controlled uptake and use of iron by plants. p. 251–266. *In* J.A. Manthey, D.E. Crowley, and D.G. Luster (ed.) Biochemistry of metal micronutrients in the rhizosphere. Lewis Publ., Boca Raton, FL.

Jordan, C.F. 1969. Derivation of leaf area index from quality of light on the forest floor. Ecology 50:663–666.

Kim, M.S., C.S.T. Daughtry, E.W. Chappelle, J.E. McMurtrey III, and C.L. Walthall. 1994. The use of high spectral resolution bands for estimating absorbed photosynthetically active radiation (Apar). p. 299–306. *In* Proc. Symp. on Physical Measurements and Signatures in Remote Sensing, 6th, Val D'Isere, France. 17–21 Jan. 1994. ISPRS Commission VII WG I, CNES, Paris.

Lichtenthaler, H.K., M. Lang, M. Sowinska, F. Heisel, and J.A. Mieh. 1996. Detection of vegetation stress via a new high resolution fluorescence imaging system. J. Plant Physiol. 148:599–612.

Lillesaeter, O. 1982. Spectral reflectance of partly transmitting leaves: Laboratory measurements and mathematical modelling. Remote Sens. Environ. 12:247–254.

Marschner, H., V. Romheld, and M. Kissel. 1986. Different strategies in higher plants in mobilization and uptake of iron. J. Plant Nutr. 9:695–713.

Miller, J.R., E.W. Hare, and J. Wu. 1990. Quantitative characterization of the vegetation red edge reflectance: An inverted-Gaussian model. Int. J. Remote Sens. 11:1755–1773.

Nakano, H., A. Makino, and T. Mae. 1997. The effect of elevated partial pressures of CO_2 on the relationship between photosynthetic capacity and N content in rice leaves. Plant Physiol. 115:191–198.

Peñuelas, J., I. Filella, P. Lloret, F. Muñoz, and M. Vilajeliu. 1995. Reflectance assessment of mite effects on apple trees. Int. J. Remote Sens. 16:2727–2733.

Peñuelas, J., J.A. Gamon, A.L. Fredeen, J. Merino, and C.B. Field. 1994. Reflectance indices associated with physiological changes in nitrogen- and water-limited sunflower leaves. Remote Sens. Environ. 48:135–146.

Peñuelas, J., J. Piñol, R. Ogaya, and I. Filella. 1997. Estimation of plant water concentration by the reflectance Water Index (R900/R970). Int. J. Remote Sens. 18:2869–2875.

Plant, R.E., D.S. Munk, B.R. Roberts, R.L. Vargas, D.W. Rains, R.L. Travis, and R.B. Hutmacher. 2000. Relationships between remotely sensed reflectance data and cotton growth and yield. Trans. ASAE 43(3):535–546.

Qi, J., A. Chehbouni, A.R. Huete, Y.H. Keer, and S. Sorooshian. 1994. A modified soil vegetation adjusted index. Remote Sens. Environ. 48:119–126.

Rejesus, R.M., and R.H. Hornbaker. 1999. Economic and environmental evaluation of alternative pollution-reducing nitrogen management practices in central Illinois. Agric. Ecosyst. Environ. 75: 41–53.

Richards, J.A. 1994. Remote sensing digital image analysis. An introduction. 2nd ed. Springer-Verlag, Heidelberg, Germany.

Rock, B.N., T. Hoshizaki, and J.R. Miller. 1988. Comparison of in situ and airborne spectral measurements of the blue shift associated with forest decline. Remote Sens. Environ. 24:109–127.

Rondeaux, G., M. Steven, and F. Baret. 1996. Optimization of soil-adjusted vegetation indices. Remote Sens. Environ. 55:95–107.

Rougean, J.-L., and F.M. Breon. 1995. Estimating PAR absorbed by vegetation from bidirectional reflectance measurements. Remote Sens. Environ. 51:375–384.

Rouse, J.W., R.H. Haas, J.A. Schell, D.W. Deering, and J.C. Harlan. 1974. Monitoring the vernal advancements and retrogradation of natural vegetation. NASA/GSFC, Greenbelt, MD.

Running, S.W., D.D. Baldocchi, D.P. Turner, S.T. Gower, P.S. Bakwin, and K.A. Hibbard. 1999. A global terrestrial monitoring network integrating tower fluxes, flask sampling, ecosystem modeling and EOS satellite data. Remote Sens. Environ. 70:108–127.

Schröder, J.J., J.J. Neeteson, O. Oenema, and P.C. Struik. 2000. Does the crop or the soil indicate how to save nitrogen in maize production? Reviewing the state of the art. Field Crops Res. 66:151–164.

Schulze, E.D., W. De Vries, and M. Hauhs. 1989. Critical loads for nitrogen deposition in forest ecosystems. Water Air Soil Pollut. 48:451–456.

Sellers, P.J., Y. Mintz, Y.C. Sud, and A. Dalcher. 1986. A simple biosphere model (SiB) for use within general circulation models. J. Atmos. Sci. 43:505–531.

Sims, D.A., and J.A. Gamon. 2002. Relationships between leaf pigment content and spectral reflectance across a wide range of species, leaf structures and developmental stages. Remote Sens. Environ. 81 (2–3):337–354.

Sims, D.A., and J.A. Gamon. 2003. Estimation of vegetation water content and photosynthetic tissue area from spectral reflectance: A comparison of indices based on liquid water and chlorophyll absorption features. Remote Sens. Environ. 84(4):526–537.

Tagliavini, M., and A.D. Rombolà. 2001. Iron deficiency and chlorosis in orchard and vineyard ecosystems. Eur. J. Agron. 15:71–92.

Tou, J.T., and R.C. González. 1974. Pattern recognition principles. Addison-Wesley Publ. Co., Reading, MA.

[USDA-NRCS] USDA Natural Resources Conservation Service. 1978. Soil Survey Kings County, California. USDA Soil Conserv. Serv. U.S. Gov. Print. Office, Washington, DC.

Ustin, S.L., D.A. Roberts, J. Pinzon, S. Jacquemoud, M. Gardner, G. Scheer, C.M. Castañeda, and A. Palacios-Orueta. 1998. Estimating canopy water content of chaparral shrubs using optical methods. Remote Sens. Environ. 65:280–291.

Varvel, G.E., J.S. Schepers, and D.D. Francis. 1997. Ability of in-season correction of nitrogen deficiency in corn using chlorophyll meters. Soil Sci. Soc. Am. J. 61:1233–1239.

Vogelmann, J.E., B.N. Rock, and D.M. Moss. 1993. Red edge spectral measurements from sugar maple leaves. Int. J. Remote Sens. 14: 1563–1575.

Wallace, A. 1991. Rational approaches to control of iron deficiency other than plant breeding and choice of resistant cultivars. Plant Soil 130:281–288.

Wiegand, C.L., A.J. Richardson, D.E. Escobar, and A.H. Gerbermann. 1991. Vegetation indices in crop assessments. Remote Sens. Environ. 35(1):105–119.

Willis, P.R., P.G. Carter, and C.J. Johansen. 1999. Assessing yield parameters by remote sensing techniques. p. 1413–1422. *In* P.C. Robert et al. (ed.) Precision agriculture. Proc. Int. Conf., 4th, St. Paul, MN. 19–22 July 1998. ASA, CSSA, and SSSA, Madison, WI.

Wood, C.W., D.W. Reeves, and D.G. Himelrick. 1993. Relationships between chlorophyll meter readings and leaf chlorophyll concentration, N status, and crop yield: A review. Proc. Agron. Soc. N. Z. 23:1–9.

Woodrow, I.E., and J.A. Berry. 1988. Enzymatic regulation of photosynthetic CO_2 fixation in C_3 plants. Annu. Rev. Plant Physiol. Plant Mol. Biol. 39:533–594.

Yang, C., J.M. Bradford, and C.L. Wiegand. 2001. Airborne multispectral imagery for mapping variable growing conditions and yields of cotton, grain sorghum, and corn. Trans. ASAE 44(6):1983–1994.

Yang, C., and J.H. Everitt. 2002. Relationships between yield monitor

data and airborne multidate multispectral digital imagery for grain sorghum. Precis. Agric. 3:373–388.

Yang, C., S.M. Greenberg, J.H. Everitt, T.W. Sappington, and J.W. Norman, Jr. 2003. Evaluation of cotton defoliation strategies using airborne multispectral imagery. Trans. ASAE 46(3):869–876.

Yoder, B.J., and R.E. Pettigrew-Crosby. 1995. Predicting nitrogen and chlorophyll content and concentrations from reflectance spectra (400–2500 nm) at leaf and canopy scales. Remote Sens. Environ. 53:199–211.

Yuzhu, L. 1990. Estimating production of winter wheat by remote sensing and unified ground network: II. Nationwide estimation of wheat yields. p. 149–158. *In* M.D. Steven and J.A. Clark (ed.) Applications of remote sensing in agriculture. Butterworths, London.

Zarco-Tejada, P.J. 2000. Hyperspectral remote sensing of closed forest canopies: Estimation of chlorophyll fluorescence and pigment content. Ph.D. diss. Graduate Program in Earth and Space Sci., York Univ., Toronto, ON, Canada.

Zarco-Tejada, P.J., J.R. Miller, G.H. Mohammed, and T.L. Noland. 2000. Chlorophyll fluorescence effects on vegetation apparent reflectance: I. Leaf-level measurements and simulation of reflectance and transmittance spectra. Remote Sens. Environ. 74(3):582–595.

Zarco-Tejada, P.J., J.R. Miller, G.H. Mohammed, T.L. Noland, and P.H. Sampson. 1999. Canopy optical indices from infinite reflectance and canopy reflectance models for forest condition monitoring: Application to hyperspectral CASI data. *In* IEEE 1999 Int. Geosci. and Remote Sensing Symp., IGARSS'99, Hamburg, Germany. 28 June–2 July 1999. Proc. of the IEEE, Piscataway, NJ.

Zarco-Tejada, P.J., J.R. Miller, G.H. Mohammed, T.L. Noland, and P.H. Sampson. 2001. Scaling-up and model inversion methods with narrow-band optical indices for chlorophyll content estimation in closed forest canopies with hyperspectral data. IEEE Trans. Geosci. Remote Sens. 39(7):1491–1507.

Zarco-Tejada, P.J., C.A. Rueda, and S.L. Ustin. 2003. Water content estimation in vegetation with MODIS reflectance data and model inversion methods. Remote Sens. Environ. 85(1):109–124.